A SPH simulation method for opening flow of fresh concrete considering boundary restraint

Guodong Cao, Zhuguo Li *, Zhisong Xu

Graduate School of Science and Technology for Innovation, Yamaguchi University, Ube, Yamaguchi, Japan

HIGHLIGHTS

- Mechanism of boundary restraint on fresh concrete was clarified theoretically.
- A boundary restraint stress model was proposed for fresh concrete's opening flow.
- Flow of fresh concrete between steel bars was simulated by SPH and VGM model.
- Effects of steel bars' gap were clarified on concrete's opening flow behaviors.

ARTICLE INFO

ABSTRACT

When fresh concrete flows through opening, such as steel bars, blockage may occur due to segregation or insufficient fluidity. Insufficient fluidity may be attributed to the increase of deformation resistance because of opening's boundary restraint. In this paper, opening flow behavior of fresh concrete was analyzed by Smoothed Particle Hydrodynamics. We proposed a boundary restraint stress model to treat opening's boundary restraint to the flow, which clarified that normal stress acting on the shear plane of fresh concrete increases during opening flow. The parameters in the model were obtained by matching the experimental and numerical results of V-funnel flow test. Then, the flow of fresh concrete in L-box with steel bars was simulated. The numerical results indicated that the restraint of opening's boundary has considerable effect on the flow behavior when fresh concrete has larger average particle contact angle and average particle friction angle, or the opening is narrow.

© 2018 Elsevier Ltd. All rights reserved.

1. Introduction

Concrete structure is generally reinforced by steel bars. Blockage is easy to happen at the position of steel bars, if fresh concrete has low flow ability or low segregation resistance. Hence, passing ability is an important property for concrete construction, and it is necessary to study the flow behavior of fresh concrete passing through steel bars. Obviously, the passing ability is closely related to the fluidity and the segregation resistance, not an independent property of fresh concrete. High flow ability is indispensable for its flow through narrow gaps of steel bars. J-ring test is usually used to evaluate the passing ability together with the fluidity of fresh concrete [1]. However, since the gap of J-ring's bars is fixed, the test result would be used to compare the passing ability of different concrete mixtures, but it does not represent actual passing

ability during reinforced concrete placement. With the development of computer technology, numerical approach has been becoming a powerful, labor and time saving tool to reproduce the flow behaviors of fresh concrete.

Present computational models of fresh concrete were summarized by Roussel et al. [2]. Fresh concrete is usually regarded as a viscous fluid with a yield stress, most flow simulations in the past literature have used Bingham model to describe its constitutive law [3–9]. Bingham model describes shear stress (τ) as a linear function ($\tau = \tau_0 + \eta_b \gamma$) of shear strain rate γ, in which yield stress τ_0 and plastic viscosity η_b are constants. However, fresh concrete is a kind of viscous granular material with both fluid and granular characteristics, rather than a purely viscous fluid [10]. It is not doubtful that there are inter-particle friction and particle interlocking in fresh concrete, which cause the vertical pressure–dependence of fresh concrete and affect its flow behaviors. High fluidity concrete has relatively obvious fluid characteristic, Bingham model may be roughly applied to it, but for ordinary concrete, the application of Bingham model is an issue. The Viscous Granular

---

* Corresponding author.
  E-mail address: li@yamaguchi-u.ac.jp (Z. Li).

Nomenclature

a, b	parameters of boundary restraint stress model (Eq. (12))	*Greek letters*	
d_s	shear thickness	$\dot{\gamma}$	shear strain rate
C_{w1}	shear resistance caused by the surface tension and suction effect of mixing water	γ_0	shear strain limit
		$\gamma_f, \dot{\gamma}_f$	shear strain limit and shear strain rate at the shear failure point, respectively
$f(x)$	arbitrary field function		
g	gravitational acceleration	γ_i	shear deformation of particle i
h	smoothing length	ε	normal strain
I	unit matrix	ε_i	vertical deformation of particle i
m	mass of particle	η	essential viscosity
n	number of moving particles in a shear plane with unit dimension	η_b	plastic viscosity
		θ_f, θ_i	average particle contact angle and contact angle of particle i, respectively
p	hydrostatic pressure at equilibrium	κ	a parameter related to shearing time-dependence
P	total stress tensor	Λ	average moving distance of moving particles
q	parameters in kernel equation	Λ_i	moving distance of particle i
s	displacement of particle in flow direction	ρ	density of particle
t_f	shearing time before entering shear failure state	σ_n	normal stress acting on the maximum shear plane
r	distance between two particles	σ_{n0}	initial normal stress caused by self-gravity of concrete sample
t	time		
v	velocity of particle	τ	shear stress
W	kernel function	τ_0	yield stress
		τ_f	shear failure limit stress
		ϕ	average inter-particle frictional angle

Materials (VGM) model was proposed to describe the nonlinear, time and pressure-dependent characteristics of fresh concrete [11]. A new numerical method has been developed by the authors, using Smoothed Hydrodynamics (SPH) and VGM model. With this numerical approach, the L-box flow was precisely simulated [12]. It is concluded that the VGM model can yield more precise numerical results, compared with Bingham model when the fluidity of fresh mixed cementitious materials is low.

The flow of fresh concrete is dilatant flow due to the existence of particle contact angle. When fresh concrete flows through opening or in pump pipe, the dilatant deformation is restricted by flow boundary, an additional normal stress is thus generated, as shown in Fig. 1. The additional normal stress will cause an increase of flow resistance due to the increase of inter-particle friction, etc., even result in blockage at openings [13]. Li [14] investigated experimentally the change of normal stress with shear strain of fresh concrete with a shear box, of which the deformation in vertical direction

was restrained, and then proposed a normal stress– shear strain relational equation.

V-funnel test and L-box with steel bars test are usually used to evaluate the fluidity and the filling ability of fresh concrete, respectively. The flow in these tests is restricted in some zones by flow boundary. Waarde et al. conducted two dimensional (2D) simulation of the V-funnel test of fresh concrete, using the Bingham model and not considering the slippage resistance on the flow boundaries [15]. The obtained numerical results are not well consistent with their experimental results. The difference between the numerical and experimental results was larger for the concrete with water-cement ratio (w/c) of 0.41, compared to the concretes with w/c of 0.43 and 0.45. Lashkarbolouk et al. also performed the simulation of the V-funnel test of self-consolidating concrete (SCC), using the 2D SPH [6]. Because of the 2D SPH and the assumption of homogeneous fluid, the numerical predictions were lower than the experimental results. Alyhya et al. developed 2D
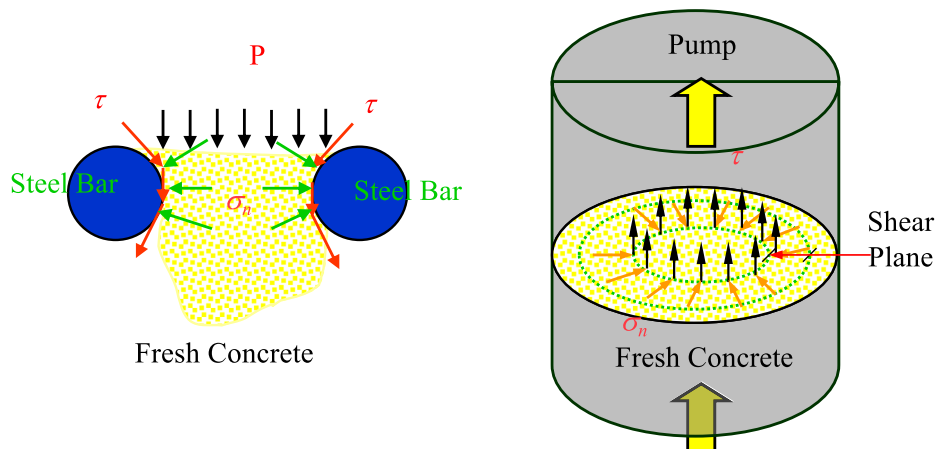

Fig. 1. Normal stress increases in restricted flow process of fresh concrete.

and 3D SPH methods to simulate the V-funnel flow of SCC [9]. They confirmed that numerical simulation results of outflow time, using 3D SPH method, were very agreeable with those recorded in the test. In contrast, 2D SPH method gave a shorter outflow time than the experimental result.

Hosseinpoor et al. performed the flow simulation of L-box using a Flow3D software to investigate the effects of steel bars' gap and coarse aggregate content on the flow blockage and the segregation of SCC [16]. AL-Rubaye et al. used the 3D SPH and the Bingham model to simulate the flow behaviors of SCC in the L-box [9]. The good agreement of numerical flow simulation with actual L-box flow revealed that the proposed approach is very well applied to SCC. Deeb et al. employed SPH to simulate the flow of SCC with or without steel fibres in the L-box to examine the distribution and orientation of fibres [4]. However, the boundary restraint to the flow of fresh concrete is not considered in these simulations.

Fresh concrete is essentially a particle assembly containing water. Particle-based Lagrangian numerical approach to the flow simulation of fresh concrete is simpler and more appropriate than the mesh-based methods that may adapt to small deformation simulation. In this study, we first proposed a boundary restraint stress model for describing the effect of boundary restraint on flow resistance, then presented a new 3D SPH, using the VGM model and the boundary restraint stress model, to simulate opening flow of fresh concrete. As an application example of this numerical method, the flow behaviors of two series of fresh concrete in L-box with steel bars were numerically investigated after the parameters of the VGM model were measured and the parameters of boundary restraint stress model were calibrated by matching the numerical and experimental results of V-funnel's outflow mass-flow time relational curve.

2. Smoothed particle hydrodynamics for opening flow

2.1. Basic SPH methodology

SPH is a particle-based numerical approach, in which the fluid continuum is discretized into particles [17]. The interpolating points are the particles, which possess material properties. For an arbitrary field function $f(x)$, it is approximated by an integral interpolation.

$$f(x) \approx \int f(x')W(|x-x'|,h)\mathrm{d}x' \tag{1}$$

where, W is a kernel function, h is smoothing length. The kernel function W should satisfy three conditions: delta function property, compact condition, and normalization. There are a lot of kernel functions [18]. The popular cubic spine function was used here as follows.

$$W(q,h) = \alpha_d \begin{cases} 1 - \frac{3}{2}q^2 + \frac{3}{4}q^3 & 0 \le q \le 1 \\ \frac{1}{4}(2-q)^3 & 1 \le q \le 2 \\ 0 & q \ge 2 \end{cases} \tag{2}$$

where, $q = r/h$, r is distance between two particles.

The continuous form of kernel approximation shown in Eq. (1) can be written in a discretized form of the summation of the particles within the influence region of kernel function, as follows.

$$f(x_i) = \sum_j \frac{m_j}{\rho_j} f(x_j)W(|x_i - x_j|,h) \tag{3}$$

where m is mass of particle, ρ is density of particle.

2.2. Governing equation

Mass and momentum conversation equations are essential for SPH method.

$$\frac{d\rho}{dt} = -\rho\nabla \cdot v \tag{4}$$

$$\frac{dv}{dt} = \frac{1}{\rho}\nabla \cdot P + g \tag{5}$$

where, v is velocity of particle, t is time, P is total stress tensor, g is gravitational acceleration.

The total stress tensor P is expressed by

$$P = -pI + \tau \tag{6}$$

where, p is hydrostatic pressure at equilibrium, I is unit matrix.

2.3. Constitutive model of fresh concrete

In order to consider the effect of normal stress, resulted from the restricted dilatant deformation, on the flow of fresh concrete, the simplified VGM model was used as the constitutive model, which is expressed in Eq. (7). Details about the SPH method coupled with the VGM model can be found in Ref. [12].

$$\begin{aligned} \tau &= \begin{cases} \frac{\tau_f}{\dot{\gamma}_f}\dot{\gamma} & \tau < \tau_f \\ \tau_f^* + \eta_t\dot{\gamma} & \tau \ge \tau_f \end{cases} \\ \tau_f^* &= \sigma_n\tan(\theta_f e^{-\kappa\cdot\dot{\gamma}\cdot(t-t_f)} + \phi) + C_{w1}, \\ \eta_t &= \frac{\eta}{\cos(\theta_f e^{-\kappa\cdot\dot{\gamma}\cdot(t-t_f)})}\dot{\gamma} \\ \tau_f &= \sigma_n\tan(\theta_f + \phi) + C_{w1} \end{aligned} \tag{7}$$

where, τ_f is shear failure limit stress, $\dot{\gamma}_f$ is shear strain rate at the shear failure point, σ_n is normal stress acting on the maximum shear plane, θ_f is average particle contact angle at the shear failure point, κ is a parameter related to shearing time-dependence, t_f is shearing time before entering shear failure state, ϕ is average inter-particle frictional angle, C_{w1} is shear resistance caused by the surface tension and suction effect of mixing water, η is essential viscosity that is associated with temperature and potential energy of cement when there is no particle contact in fresh concrete.

2.4. Boundary restraint of opening flow

It is considered that granular materials dilate in response to shear deformation [19–22]. Bi et al. [23] found that the granular materials with a packing fraction of solid particles smaller than the critical value might jam together with shear deformation, i.e. negative dilatancy happens. However, when the packing fraction is above the critical value, normal stress occurs, accompanying shear deformation. Ren et al. [24] found that when a disordered disk assembly was sheared, normal stress firstly increased with the increase of shear strain. The greater the particle packing fraction, the more the increase of normal stress. Then, the normal stress approaches to a stable value, when the shear strain is above a limit. The greater the particle packing fraction, the smaller the shear strain limit. Since fresh concrete is a kind of viscous granular material too, it is a dilatant material. Li et al. [14] investigated the change of normal stress by using a shear box in the state that the deformation perpendicular to the shear plane is restricted. Based on the experimental results of normal stress-shear strain relationship shown in Fig. 2, they presented the normal stress-shear strain relational equations, as expressed by Eq. (8). Because of the constraint of shear box's structure, the maximum shear strain that
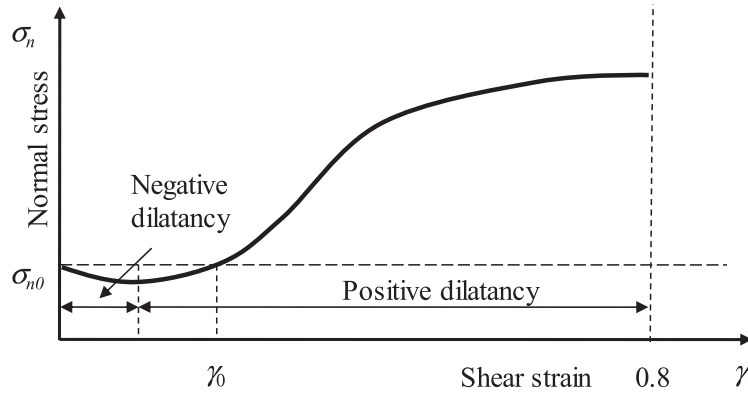
Fig. 2. The relationship of normal stress and shear strain (σ_n-γ).

could be generated was 0.8. That is to say, the Eq. (8) is valid only when shear strain is less than 0.8.

$$\sigma_n = \begin{cases} \sigma_{n0}, & 0 \leq \gamma \leq \gamma_0 \\ \sigma_{n0} - a(\gamma - \gamma_0)^2 + b(\gamma - \gamma_0), & \gamma_0 < \gamma \leq 0.8 \end{cases} \quad (8)$$

where, σ_{n0} is initial normal stress caused by self-gravity of concrete sample, γ_0 is shear strain limit from which normal stress is larger than its initial value, and a and b are constants that vary with concrete mixture.

In the initial stage of shear deformation, the contacts of part of particles are loose and the degree of particle interlocking is low. Accompanying the shear deformation caused by applied external force, some of the particles in the loose state have to move to contact tightly for resisting the external force or shear stress. Hence, negative dilatancy occurs in this stage. However, as shown in Fig. 3, negative dilatancy occurs only in the initial stage of shear flow. If fresh concrete deforms continuously, compacted particles will expand away, thus positive dilatancy happens. When fresh concrete flows into an opening, it is considered that fresh concrete's shear deformation already went through the initial stage of shear flow, only positive dilatancy occurs during flowing through the opening. Hence, in this study, we only considered the normal stress resulted from the boundary restraint to the positive dilatancy. In the following, we will discuss the change of normal stress based on the analysis of dilatant deformation.

Li et al. [13] clarified the flow mechanism of fresh concrete based on the probability theory and expanding the Eyring rate process theory. In this theory, the shear deformation of granular material is caused by particle movement. If one particle moves a distance Λ_i at a particle contact angle θ_i, the granular material or particle assembly will deform in shear direction for $\Lambda_i\cos\theta$, together with a vertical deformation $\Lambda_i \sin\theta_i$, as shown in Fig. 3.

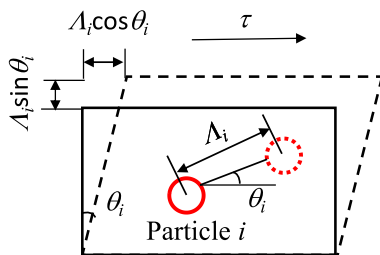$$\varepsilon_i = \Lambda_i\sin\theta_i, \gamma_i = \Lambda_i\cos\theta_i \quad (9)$$

where, ε_i is vertical deformation of particle assembly caused by movement of particle i, Λ_i is moving distance of particle i, γ_i is shear deformation of particle assembly caused by movement of particle i, θ_i is particle contact angle of particle i.

When n particles move in the particle layer, normal strain ε and shear strain γ of fresh concrete will occur, as expressed by [13].

$$\varepsilon = n\Lambda\sin\theta, \quad \gamma = n\Lambda\cos\theta \quad (10)$$

where, n is number of moving particles in a shear plane with unit dimension Λ is average moving distance of moving particles, and θ is average particle contact angle of moving particle.

Hence, the relationship between normal strain and shear strain is as expressed by Eq. (11).

$$\varepsilon = \gamma\tan\theta \quad (11)$$

Before entering into the shear failure state, in order to support the shear stress, some particles move to their new stable positions where greater inter-particle forces can be supported. The θ increases, i.e. the degree of particle interlocking rises up. And the greater the shear stress, the more moving particles. Therefore, before fresh concrete enters into the shear failure state, the normal strain increases with the increase of shear stress or shear strain. If the normal strain is restricted, there is no doubt that normal stress will increase with the growth of shear deformation.

However, when shear stress τ and shear strain γ reach to their limit values, respectively, some of the moving particles (hereafter called as failure particle) cannot find their stable positions because their inter-particle forces are so large that no position can support them. That is to say, the θ can't further increase with shear stress or shear strain, the θ reaches to its critical value θ_f. Once the failure particle occurs, fresh concrete enters into shear failure state. In the shear failure state, the failure particles will move without stoppage because they can not reach to a stable position, and their particle contact angles decrease and finally approach to zero in theory. Hence, the average particle contact angle θ of ordinary moving particles and failure particles decreases continually with shear deformation or flow [11]. However, the shear strain increases
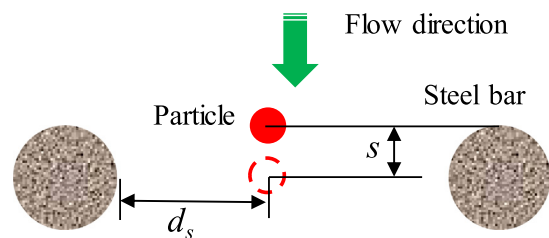

Fig. 3. Shear deformation of particle layer.

Fig. 4. Schematic diagram of fresh concrete passing through steel bars.

Table 1
Mix proportions of concrete mixtures and their slump flow values.

Series No.	w/c	SP/C (%)	Mass per unit volume (kg/m³)					S_f (mm)
			w	c	S	G	SP	
1	0.35	1.5	170	486	819	840	7.3	750
2	0.30	1.5	170	567	753	840	8.5	560

Notes: w: water, c: ordinary portland cement, S: sea sand, G: crushed stone, SP retarding type high-range water reducer, w/c: water-cement ratio, SP/C: dosage of high-range water reduce, S_f: slump flow value.

Table 2
Input parameters for the numerical simulations.

Series No.	VGM model								Boundary resistance model		Boundary restraint stress model	
	γ_f	γ_f (s⁻¹)	η (Pas)	C_{w1} (Pa)	ϕ (rad)	θ_f (rad)	κ	σ_n (Pa)	τ_{sy} (Pa)	η_s (Pa·s)	a	b
1	0.52	0.48	480	153	0.15	0.20	0.28	–	55	360	1040	1080
2	0.55	0.51	600	216	0.20	0.27	0.3	–	80	500	1100	1200
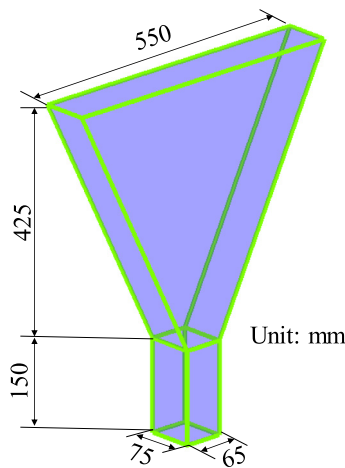
Fig. 5. Geometry of V-funnel.
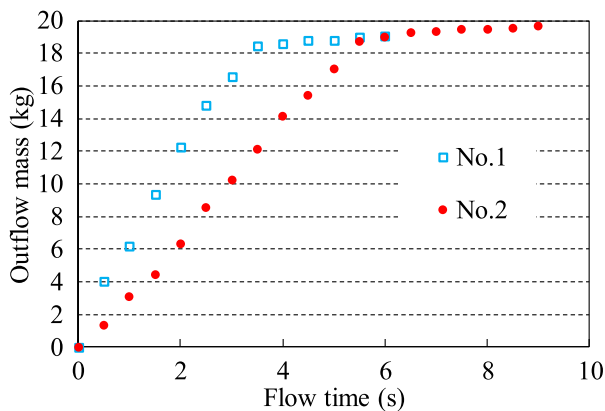
Fig. 6. Outflow mass-flow time relational curve of V-funnel flow.

(a) Without consideration of boundary restraint   (b) with consideration of boundary restraint

Fig. 7. Front side views of the flow pattern of fresh concrete of series No. 1 at two moments.

continually in the shear failure state. Hence, present theoretical analysis does not clarify the change of normal strain with shear deformation in the shear failure state.

Fig. 2 of Ref. [24] indicates that the normal stress of the sample with smaller particle packing fraction approached earlier to a stable value with the growth of shear strain. Ref. [20] shows that after the blend of silicon oil and glass beads reaches to a certain
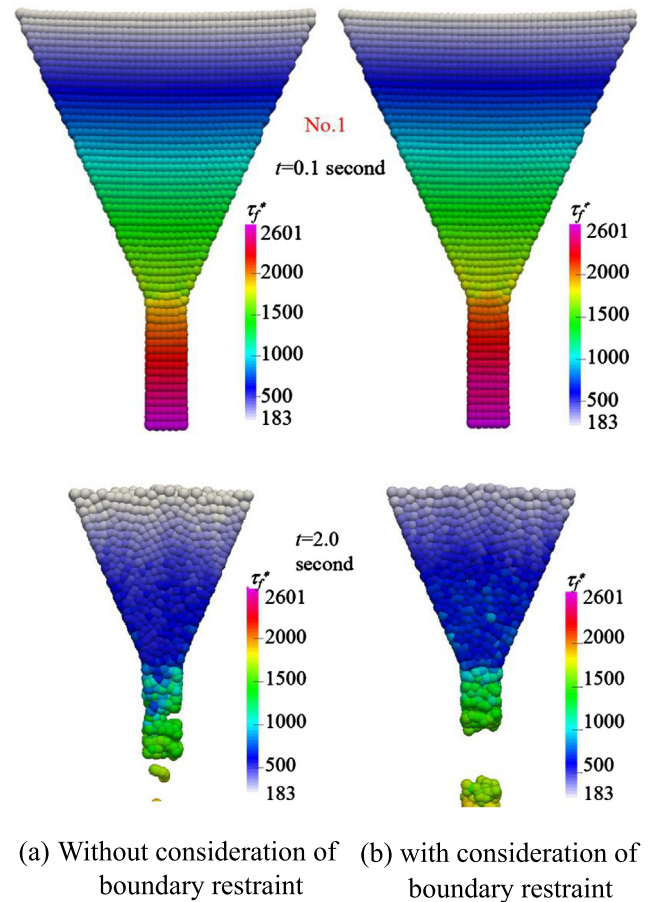
shear deformation, its normal deformation does not further increase. Though the normal stress of fresh concrete increases until shear strain of 0.8, the slope of the normal stress–shear strain relational curve becomes smaller and smaller [14]. We believe that if the shear box test can be conducted for a larger shear deformation, it is very possible to detect the stable state of normal stress. That is to say, the normal stress does not increase with shear strain when the shear strain is larger than a certain value. For the samples with

larger particle packing fraction, because their shear strains do not exceed the certain values, the normal stress gets near each stable value [14,24].

According to the above analyses on the experimental results, it is thought that after fresh concrete entered into shear failure state, its normal strain nearly does not change. Therefore, the normal stress resulted by the restraint of dilatant deformation does not change with shear strain γ. Based on Eq. (8), we proposed a boundary restraint stress model in this study, as expressed by Eq. (12).

$$\sigma_n = \begin{cases} \sigma_{n0} - a\gamma^2 + b\gamma, & \gamma < \gamma_f \\ \sigma_{n0} - a\gamma_f^2 + b\gamma_f, & \gamma \geq \gamma_f \end{cases} \tag{12}$$
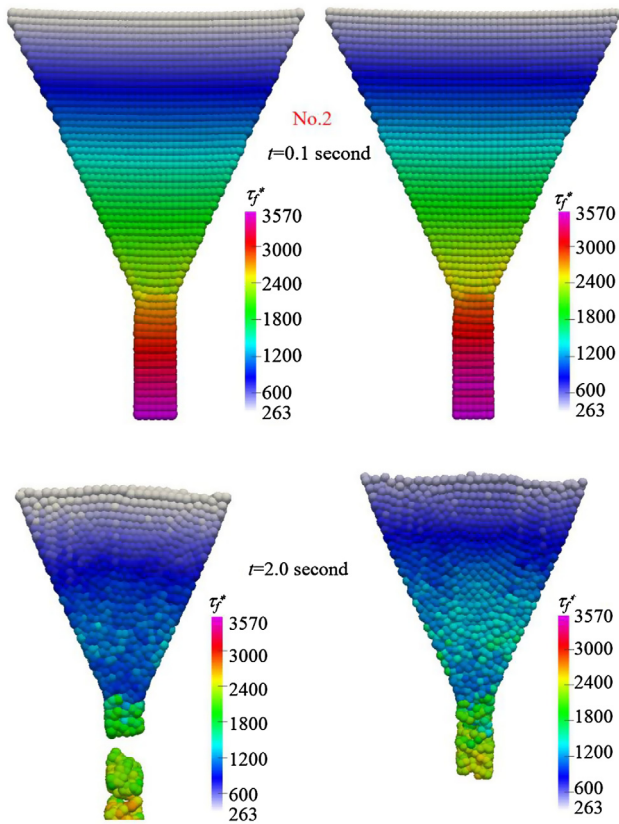
(a) Without consideration of boundary restraint   (b) with consideration of boundary restraint

Fig. 8. Front side views of the flow pattern of fresh concrete of series No. 2 at two moments.

where γ_f is shear strain limit at shear failure point.

The shear strain γ when fresh concrete passes through opening, e.g. steel bars as shown in Fig. 4 is expressed by Eq. (13).

$$\gamma = s/d_s \tag{13}$$

where, s is displacement of particle in flow direction, d_s is shear thickness which is equal to distance from the particle to opening's boundary.

According to Eq. (12), the increase of shear strain will lead to an increase of normal stress. Hence, when flowing through a narrower opening, a greater shear strain will be yielded, and accordingly a larger normal stress arises. The shear resistance increases with the increase of normal stress according to Eq. (7), the flow velocity of fresh concrete will decrease, even cause blockage.

3. Experiment

3.1. Concrete mixtures and rheological properties

Two series of fresh concrete with different water cement ratio (w/c) was planned. The mix proportions are shown in Table 1. Ordinary Portland cement with density of 3.16 g/cm^3, and specific surface area of 3500 cm^2/g was used. Coarse aggregate was continuously graded crushed stone with sizes of 5–20 mm. The sea sand with maximum size of 5 mm was employed as fine aggregate, which was washed by fresh water to have Cl$^-$ content of 0.017%. The coarse and fine aggregate had densities of 2.6 and 2.55 g/cm^3 in saturated surface dry state, fineness modulus of 6.5 and 2.8, respectively. Retarding type high-range water reducer were added.

30 L of concrete sample was prepared by a concrete mixer for each mixture. The rheological parameters of the VGM model were measured by the RSNS rheometer. The test protocol consists of torque growth and rotation speed sweep stages. The torque, rotational angle, and rotational speed of the lower blade were recorded. Details of the RSNS rheometer, test method, and calculating methods of the parameters in the VGM model can be found in Ref. [11]. The parameters in the VGM model were calculated and shown in Table 2. It should be noted that the normal stress is dependent on the self-gravity of concrete sample and the boundary restraint, as shown in Eq. (12). Therefore, it is not a constant, and should be updated according to the shear strain in vertically restricted state.

3.2. V-funnel test

V-funnel test is always used to evaluate the flow ability of fresh concrete [6,9]. The geometry of the V-funnel used in this study is shown in Fig. 5. After the concrete sample was filled into the V-funnel, the gate of funnel was opened quickly. The sample flowed
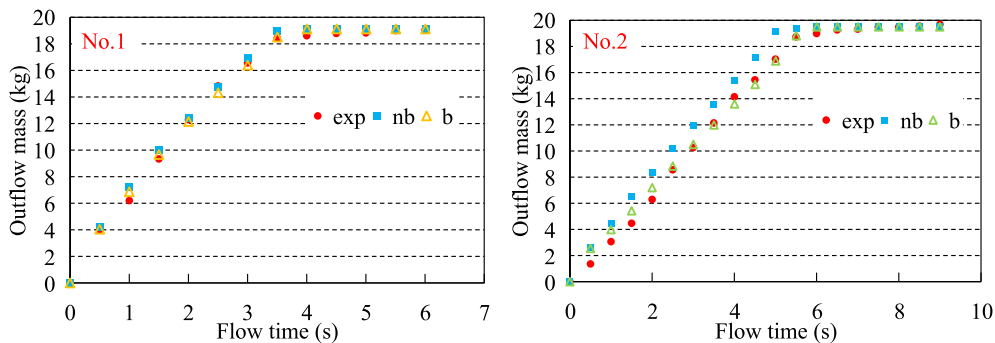

Fig. 9. Comparison of numerical and experimental results of V-funnel flow (exp: experimental result, b and nb represent the numerical results with and without consideration of boundary restraint, respectively).

down into a container located on an electronic scale, the outflow mass was measured at time interval of 0.5 s. The outflow time was recorded from the moment when the sample flowed out from the rectangular outlet. Measured outflow mass-flow time relational curves of two series of concrete are shown in Fig. 6. Series No. 1 with higher fluidity flowed faster than series No. 2 with lower fluidity, and the total outflow time of the former was shorter (about 4.0 s).

4. Numerical simulation of V-funnel

9392 material particles and 3762 boundary particles were used to represent fresh concrete and the V-funnel's wall, respectively. The diameters of material particles are 10 mm. The number of material particles was determined to ensure adequate computation accuracy in a tolerant computation time. Once a material particle flowed out from the rectangular outlet, the material particle was deleted from the numerical calculation. The input values of the parameters used in this paper are shown in Table 2.

The visco-plastic model [25], used in the authors' past study [12] to describe the boundary's slip resistance, was also used in this paper. The parameters in the visco-plastic model were set up, as shown in Table 2. The values of parameter a, b in the boundary restraint stress model (see Eq. (12)) were obtained by matching the experimental and numerical results of outflow mass-outflow time relationship of the V-funnel test. However, this parametric study method does harm the following discussion on the necessity of considering the boundary restraint.

Figs. 7 and 8 show the calculating results of particle distribution at 0.1 s and 2.0 s for the two series of fresh concrete, respectively. The color bar indicates the level of apparent yield stress (τ_f^*) in Eq. (7). The greater the normal stress, the larger the apparent yield stress. At 0.1 s of outflow time, because the shear strain of fresh concrete is small, the normal stress resulted from boundary restraint is small according to Eq. (12). Therefore, for any of the fresh concretes, no matter whether boundary restraint is considered or not, the concrete sample has almost the same distribution of τ_f^*. But the τ_f^* of series No. 2 is larger than that of series No. 1. This is because that 1) two series of fresh concrete have different densities, different self-gravity causes different normal stress, and 2) the τ_f^* and η may increase with the decrease of concrete's fluidity.

On the other hand, at 2.0 s of outflow time, for series No. 1, the sample remained in the V-funnel in case of considering the boundary restraint is almost the same with the case of ignoring the boundary restraint. In contrast, consideration of the boundary restraint yields more concrete sample of series No. 2 remained in the V-funnel, compared to the case of ignoring the boundary restraint.

Fig. 9 shows a comparison of experimental and numerical results of the outflow mass-outflow time relationship. For series No. 1, no matter whether the boundary restraint is considered or not, the numerical results are very close to the experimental results. However, for series No. 2, only when the boundary restraint is considered, numerical results become consistent with the experimental results. The neglect of boundary restraint yields greater calculating results of outflow mass than the experimental results.

In case of series No. 2 with relatively low fluidity, the θ and ϕ are large, the normal stress resulted from the restraint of dilatant deformation is large according to Eqs. (10) and (12), the τ_f^* and η are large, i.e. the boundary restraint is great. Hence, ignoring the boundary restraint will cause a greater analytical error. But for series No. 1 with relatively high fluidity, the normal stress resulted from the restraint of dilatant deformation is small, the τ_f^* and η

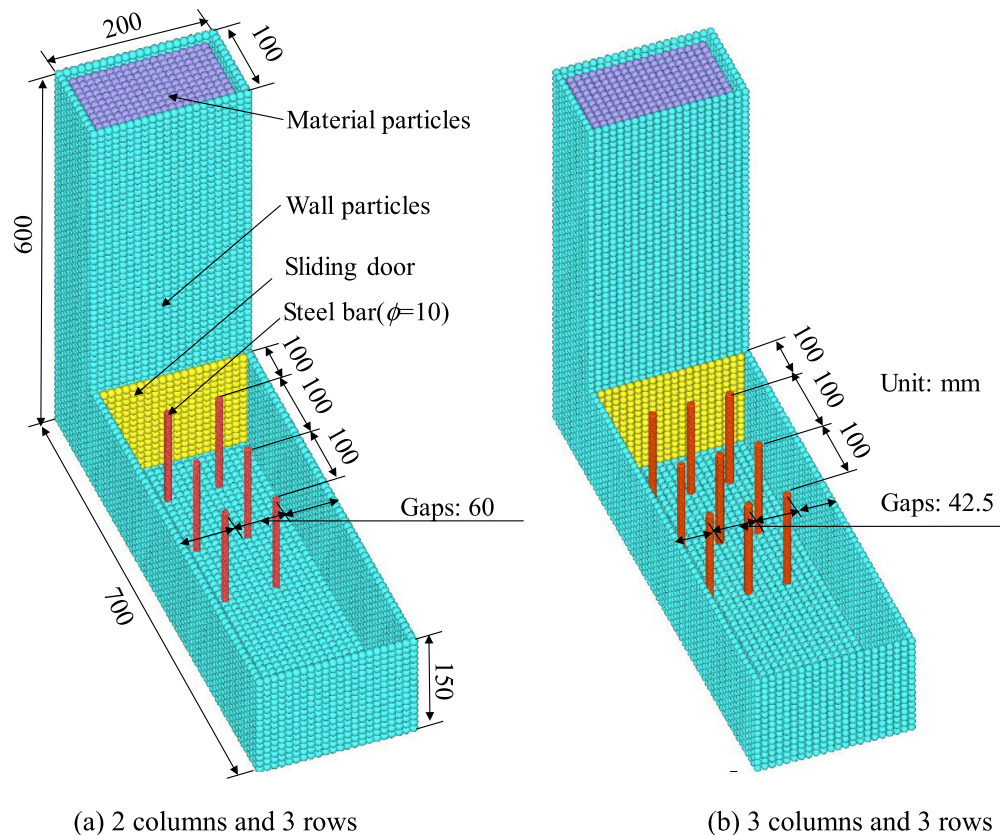(a) 2 columns and 3 rows   (b) 3 columns and 3 rows

Fig. 10. Geometry of L-box with steel bars.

are small. Thus, ignoring the boundary restraint does not produce a great difference.

5. Flow simulation of fresh concrete passing through steel bars

### 5.1. Concrete mixtures and numerical analysis conditions

The steel bars are generally used in concrete structure, which make the placement of concrete difficult. Due to the formation of arches in the entrance of opening, fresh concrete may jam between steel bars [18]. The probability of blockage of concrete increases with increasing the volume fraction of coarse aggregate or the ratio of the maximum size of coarse aggregate to the bars' gap. The development of numerical method for the flow behaviors of fresh concrete between steel bars is of significance for concrete construction. L-box with steel bars is considered to well model the placement conditions of fresh concrete. Hence, in this study we simulated the flow of fresh concrete in a L-box with steel bars, and discussed the effect of boundary restraint on the flow behaviors.

The geometry of L-box with steel bar mesh (2 columns × 3 rows or 3 columns × 3 rows) is shown in Fig. 10. The diameter of used steel bar is 10 mm, and either of the gaps between steel bars or
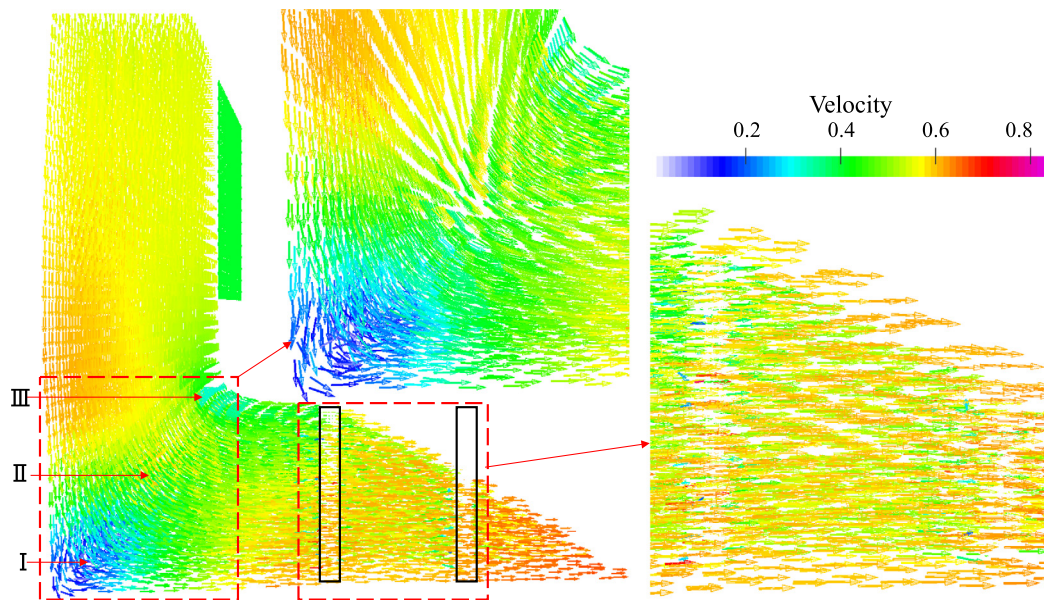
(a) Series No.1 at 0.5s
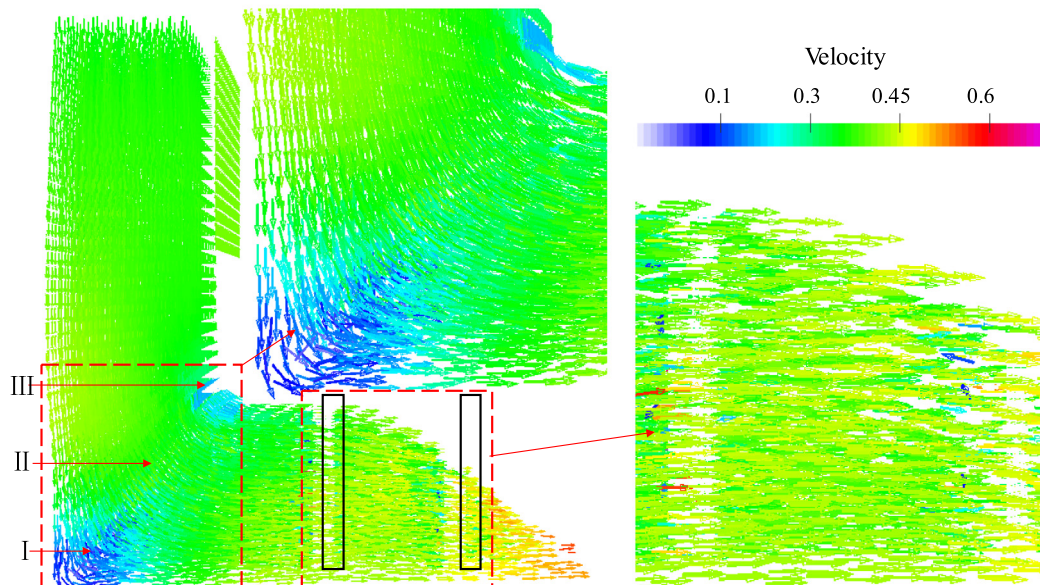
(b) Series No.1 at 0 6s

Fig. 11. Velocity vector field.

the gaps between steel bars and inside wall of box are 60 mm and 42.5 mm, respectively.

7582 wall particles and 12,980 material particles were used. The diameters of boundary and material particles are the same with those used in the numerical analysis of the V-funnel flow. Every steel bar was represented by 366 boundary particles with diameter of 2.5 mm. The L-flows of the two series of fresh concrete were simulated by using the SPH method of opening flow proposed by the authors in this study.

5.2. Numerical results and discussion

In order to examine the effect of w/c on the flow behavior of fresh concrete, the flow simulation of L-box with 2 columns × 3 rows steel bars was performed. With the consideration of boundary restraint, the velocity vector field of series No. 1 at flow time 0.5 s and series No. 2 at flow time 0.6 s is shown in Fig. 11. Why different time points were chosen is that the flow distances of the two series of concrete were almost the same at the two time points (0.5 and 0.6 s). Although the maximum velocities of both the two concretes occurred at the head of flow, at which the slope of series

No. 1 was smaller than that of series No. 2. Both of two series had the smallest velocity at the zone I. The velocity at the elbow was in the order of zone II > zone III > zone I. For a given fresh concrete, its flow velocity is dependent on its rheological properties, shear stress resulted from self-gravity, and normal stress resulted from self-gravity and boundary restraint. The series No. 1 had low viscosity and small θ_f, ϕ so that its overall velocity is larger than that of series No. 2.

Figs. 12 and 13 indicate side views of the two concretes at two flow moments (0.5 s and 2.0 s), respectively. No matter whether the restraint effect of steel bars was taken in account or not, the flow distance at 0.5 s increase with the decrease of θ_f or ϕ, but the τ_f^* at the same position of the two series decreases. The τ_f^* of the concrete, located between two steel bars arranged vertically to the flow direction, or between a steel bar and inside wall of L-box, is larger than that of the concrete flowing out of the gaps when the restraint of steel bars and wall was considered.

In order to clarify the restraint effect of steel bars, the differences ($\varDelta N$) in the numbers of material particles passing through the first row of steel bars (the closest to sliding door) without and with considering the boundary restraint effect of two series
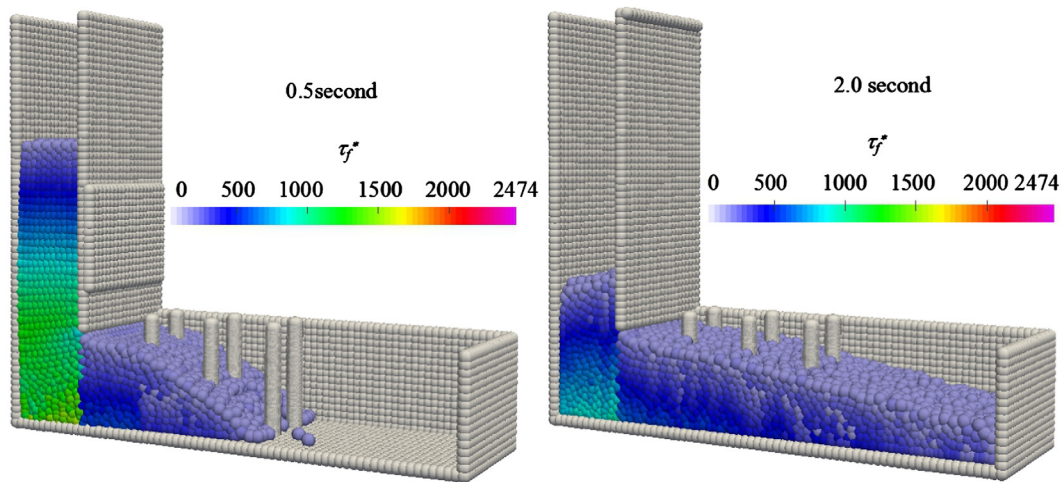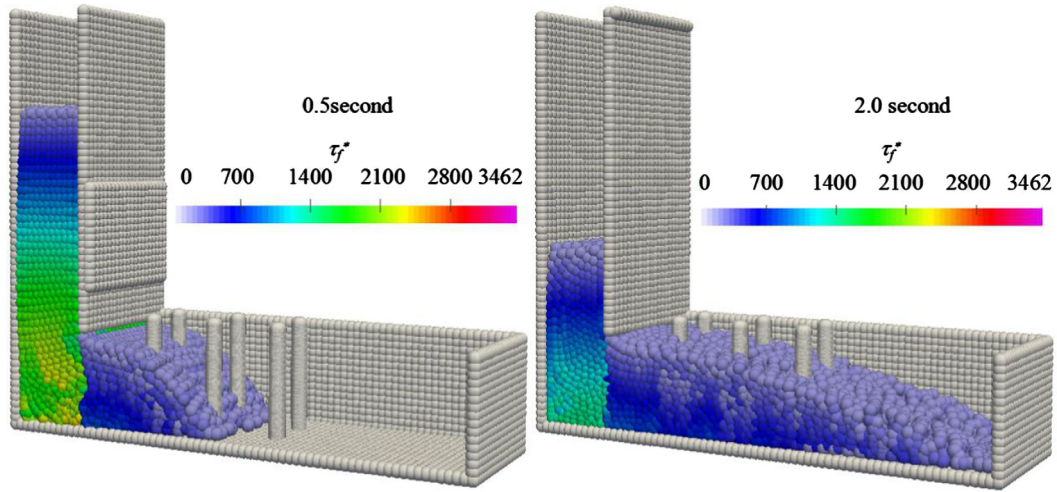

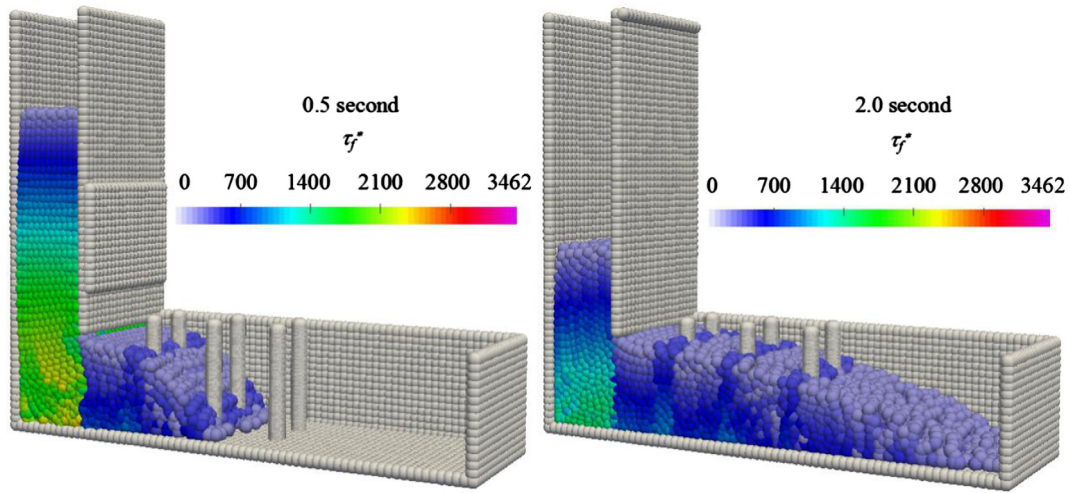
(a) Without consideration of boundary restraint
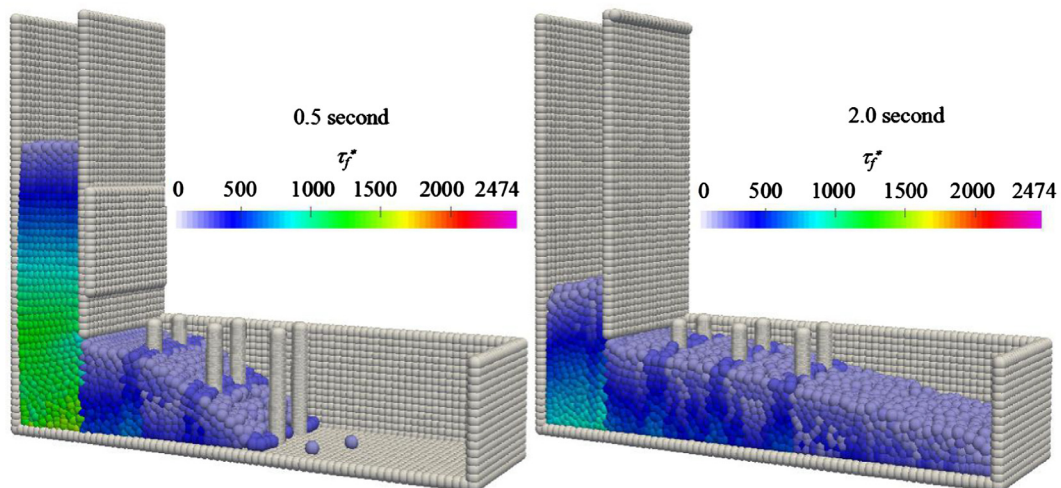
(b) With consideration of boundary restraint

Fig. 12. L-flow side views of series No. 1 at 0.5 s and 2 s.

(a) Without consideration of boundary restraint

(b) With consideration of boundary restraint

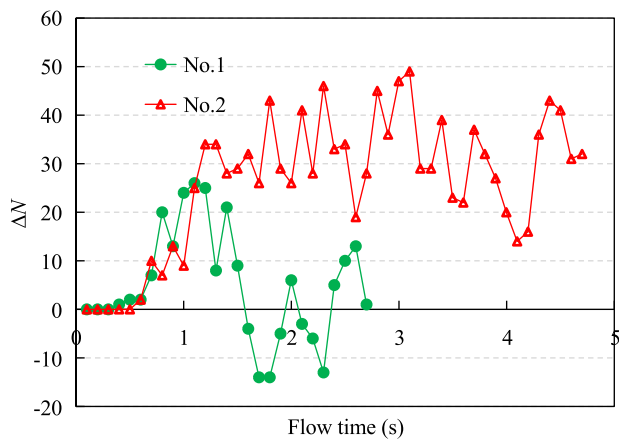**Fig. 13.** L-flow side views of series No. 2 at 0.5 s and 2 s.

Fig. 14. Differences (ΔN) in the numbers of material particles passing through the first row of steel bars (the closest to sliding door) without and with considering the restraint effect of two series of fresh concrete in case of 2 columns.
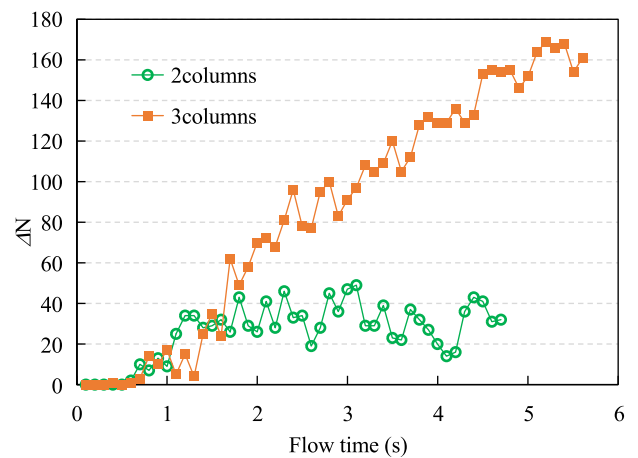

Fig. 15. ΔN of series No. 2 in case of 2 or 3 columns.

were investigated, as shown in Fig. 14. For series No. 1, the ΔN is small, that is to say, the restraint of steel bars was not obvious for high fluidity concrete with small θ_f and ϕ. The ΔN, however, became obvious when the θ_f and ϕ increase. The maximum ΔN of series No. 2 reaches to about 50.

Except for the rheological properties of fresh concrete, the gap between steel bars also affects the passing ability. The flow simulation of series No. 2 in the L-box with 3 columns × 3 rows was also conducted. As seen from Fig. 15, before about 0.6 s, the ΔN of series No. 2 in case of 2 and 3 columns are zero. This is because fresh concrete does not reach to the steel bars. After 1.0 s, due to the decrease of the gap between steel bars, the total volume of material particles which passed through the first row of steel bars in case of 2 columns is larger than that of 3 columns, thus the ΔN of the former is larger than that of the latter. With the advance of flow time, more and more material particles pass through steel bars, of which the restraint effect is dominant, the ΔN in case of 3 columns is greater than that of 2 columns after 1.8 s. The maximum ΔN in case of 3 columns is about 4 times of that in case of 2 columns at last.

6. Conclusions

Passing ability is an important factor of influencing the placement of reinforced concrete. Numerical simulation is applicable to the visualization of flow behaviors of fresh concrete when it passes through openings. However, how to treat the effect of boundary, such as mould wall and steel bars in the flow simulation of fresh concrete is an issue. In this study, the authors developed a new SPH method to simulate opening flow of fresh concrete. The VGM model shown in Eq. (7) was used to represent the constitutive model of fresh concrete, and the boundary restraint stress model shown in Eq. (12) was proposed to express the effect of boundary restraint on the flow.

Using this new SPH method, V-funnel flows of two series of concrete were simulated. The comparison of numerical and experimental results of outflow mass-outflow time relationship revealed that for the fresh concrete with low fluidity, it is needed to consider the restraint effect of boundary, ignoring the restraint effect yielded a higher outflow speed than the experimental value. Through matching the numerical and experimental results of outflow mass-outflow time relationship, the values of parameter a, b in the boundary restraint stress model can be obtained.

The flow simulations of two series of fresh concrete in L-box with steel bars were performed, and the numbers of material particles passing through the first row of steel bars were compared. Numerical results indicate that the flow behaviors are different from fresh concretes with different rheological properties. Also, for fresh concrete with lower fluidity, the restraint effect of boundary becomes remarkable. When the gap between steel bars becomes small, the restraint effect of boundary becomes obvious. Thus, the restraint action of boundary should be taken into account for doing a precise flow simulation.

Conflict of interest

None.

References

[1] W. Zhu, J.C. Gibbs, Use of different limestone and chalk powders in self-compacting concrete, Cem. Concr. Res. 35 (8) (2005) 1457–1462.

[2] N. Roussel, M.R. Geiker, F. Dufour, et al., Computational modeling of concrete flow: general overview, Cem. Concr. Res. 37 (9) (2007) 1298–1307.

[3] R. Deeb, S. Kulasegaram, B.L. Karihaloo, 3D modelling of the flow of self-compacting concrete with or without steel fibres part I: slump flow test, Comput. Part. Mech. 1 (4) (2014) 373–389.

[4] R. Deeb, S. Kulasegaram, B.L. Karihaloo, 3D modelling of the flow of self-compacting concrete with or without steel fibres part II: L-box test and the assessment of fibre reorientation during the flow, Comput. Part. Mech. 1 (4) (2014) 391–408.

[5] S. Kulasegaram, B.L. Karihaloo, Fibre-reinforced, self-compacting concrete flow modelled by smooth particle hydrodynamics, Proc. Inst. Civil Eng.-Eng. Comput. Mech. 166 (1) (2013) 22–31.

[6] H. Lashkarbolouk, A.M. Halabian, M.R. Chamani, Simulation of concrete flow in V-funnel test and the proper range of viscosity and yield stress for SCC, Mater. Struct. 47 (10) (2014) 1729–1743.

[7] M. AL-Rubaye, S. Kulasegaram, B.L. Karihaloo, Simulation of self-compacting concrete in an L-box using smooth particle hydrodynamics, Mag. Concr. Res. 69 (12) (2017) 618–628.

[8] M.A. Dhaheer, S. Kulasegaram, B. Karihaloo, Simulation of self-compacting concrete flow in the J-ring test using smoothed particle hydrodynamics (SPH), Cem. Concr. Res. 89 (2016) 27–34.

[9] W. Alyhya, S. Kulasegaram, B. Karihaloo, Simulation of the flow of self-compacting concrete in the V-funnel by SPH, Cem. Concr. Res. 100 (2017) 47–59.

[10] Z. Li, J. Li, Granular material characteristic of fresh concrete, Proc. 6th Int. RILEM Symp. Self-Compacting Concr. (2010) 423–433.

[11] Z. Li, Rheological model and rheometer of fresh concrete, J. Struct. Constr. Eng. Trans. Archit. Inst. Japan 80 (710) (2015) 527–537.

[12] G. Cao, Z. Li, Numerical flow simulation of fresh concrete with viscous granular material model and smoothed particle hydrodynamics, Cem. Concr. Res. 100 (2017) 263–274.

[13] Z. Li, T. Ohkubo, Y. Tanigawa, Flow performance of high-fluidity concrete, J. Mater. Civ. Eng. 16 (6) (2004) 588–596.

[14] J. Li, Z. Li, Effect of boundary restraint on the flow of fresh concrete through opening, J. Struct. Constr. Eng., Trans. Archit. Inst. Japan 76 (666) (2011) 1367–1374.

[15] F. Waarde, E. Koenders, J. Lycklama, et al., Theoretical and practical investigations on SCC formwork, in: Fifth international RILEM symposium on self-compacting concrete. Belgium, Sep, 2007, pp. 3–5.

[16] M. Hosseinpoor, K.H. Khayat, A. Yahia, Numerical simulation of self-consolidating concrete flow as a heterogeneous material in L-Box set-up: coupled effect of reinforcing bars and aggregate content on flow characteristics, Mater. Struct. 50 (2) (2017) 163.

[17] G.-R. Liu, M.B. Liu, Smoothed Particle Hydrodynamics: A Meshfree Particle Method, World Scientific, 2003.

[18] F. Chevoir, F. Gaulard, N. Roussel, Flow and jamming of granular mixtures through obstacles, EPL (Europhys. Lett.) 79 (1) (2007) 14001.

[19] O. Reynolds, LVII. On the dilatancy of media composed of rigid particles in contact. with experimental illustrations, London, Edinburgh Dublin Philos. Mag. J. Sci. 20 (127) (1885) 469–481.

[20] Z. Li, Y. Tanigawa, Investigation on granular characteristics of fresh concrete based on visualized experiment using alternative materials, J. Struct. Constr. Eng., Trans. Archit. Inst. Japan 77 (678) (2012) 1175–1184.

[21] M. Hyodo, Y. Wu, N. Aramaki, et al., Undrained monotonic and cyclic shear response and particle crushing of silica sand at low and high pressures, Can. Geotech. J. 54 (2) (2016) 207–218.

[22] Y. Wu, N. Yoshimoto, M. Hyodo, et al., Evaluation of crushing stress at critical state of granulated coal ash in triaxial test, Géotechnique Lett. 4 (4) (2014) 337–342.

[23] D. Bi, J. Zhang, B. Chakraborty, et al., Jamming by shear, Nature 480 (7377) (2011) 355.

[24] J. Ren, J.A. Dijksman, R.P. Behringer, Reynolds pressure and relaxation in a sheared granular system, Phys. Rev. Lett. 110 (1) (2013) 018302.

[25] J. Murata, K. Suzuki, Study on grout flow in pipe with slip at wall, Jpn. Soc. Civ. Eng. 38 (7) (1987) 129–136.